Intra-operative brain tumor detection using elastic light single-scattering spectroscopy: a feasibility study

Murat Canpolat
Akdeniz University
School of Medicine
Department of Biophysics
Antalya, 07059
Turkey

Mahmut Akyüz
Akdeniz University
School of Medicine
Department of Neurosurgery
Antalya 07059
Turkey

Güzide Ayşe Gökhan
Elif İnanç Gürer
Akdeniz University
School of Medicine
Department of Pathology
Antalya, 07059
Turkey

Recai Tuncer
Akdeniz University
School of Medicine
Department of Neurosurgery
Antalya 07059
Turkey

Abstract. We have investigated the potential application of elastic light single-scattering spectroscopy (ELSSS) as an adjunctive tool for intraoperative rapid detection of brain tumors and demarcation of the tumor from the surrounding normal tissue. Measurements were performed on 29 excised tumor specimens from 29 patients. There were 21 instances of low-grade tumors and eight instances of high-grade tumors. Normal gray matter and white matter brain tissue specimens of four epilepsy patients were used as a control group. One low-grade and one high-grade tumor were misclassified as normal brain tissue. Of the low- and high-grade tumors, 20 out of 21 and 7 out of 8 were correctly classified by the ELSSS system, respectively. One normal white matter tissue margin was detected in a high-grade tumor, and three normal tissue margins were detected in three low-grade tumors using spectroscopic data analysis and confirmed by histopathology. The spectral slopes were shown to be positive for normal white matter brain tissue and negative for normal gray matter and tumor tissues. Our results indicate that signs of spectral slopes may enable the discrimination of brain tumors from surrounding normal white matter brain tissue with a sensitivity of 93% and specificity of 100%. [DOI: 10.1117/1.3247151]

Keywords: Light; Scattering; Spectroscopy; biomedical optics; Medicine.

Paper 08146RRR received May 3, 2008; revised manuscript received Jul. 29, 2009; accepted for publication Aug. 4, 2009; published online Oct. 14, 2009.

1 Introduction

Currently, the most common treatment of brain tumors is surgical resection. Precise definition of the surgical margins prevents recurrence and increases the survival of patients. Complete resection of tumors without the sacrifice of patients' neurological functions is essential for patients' quality of life. The extent of tumor resection correlates with the prevention of recurrence, but visually differentiating normal brain tissue and the tumor during surgery is difficult.

The standard in intraoperative neuropathologic specimen evaluation is the frozen-section technique. However, processing frozen sections takes an average of 20 min. Intraoperative surgical navigation systems with registration of magnetic resonance and computed tomography images can also be used to locate tumors. However, these systems do not provide real-time imaging and the surgeon has no flexibility to investigate excised tissue margins using these techniques. Ultrasonography (US) has also been used as a real-time imaging system in neurosurgery to probe tumor margins. Intraoperative US-based surgical guidance is limited by image quality and the difficulty of image interpretation due to the unfamiliarity of image planes and interference from blood and air bubbles within the surgical field.[1,2] Spectroscopic techniques, such as fluorescence spectroscopy,[3–7] diffuse reflectance spectroscopy,[8] and a combination of diffuse reflectance and fluorescence spectroscopy,[9,10] have been used for intraoperative tumor identification or demarcation of the tumor from nontumoral brain tissue *in vivo* and *in vitro*. In some of the fluorescence tissue characterization studies, time-resolved parameters[5] or autofluorescence emission spectra[4] of UV excitation have been used for tumor demarcation. Exogenous fluorescence molecules, such as fluorescein[11] or 5-Aminolevulinic[7] acid, a precursor of protoporphoryn IX, have also been used to enhance the contrast between the tumor and the surrounding normal tissue for better identification of malignant gliomas. Light-scattering spectroscopy has also been used by several groups to obtain information about tissue for diagnostic purposes.[12–16] With current spectroscopic techniques, light is delivered with one source fiber to the tissue and detected with another fiber.[14,17] Because detected photons undergo multiple scattering events, the spectrum of the detected light reflects both scattering and absorption properties of the surrounding tissue. The spectrum of the diffused light from the source fiber to the detection fiber depends on absorption and scattering of the light by tissue. Deviations in the spectra of normal tissue may be caused by either varia-

Address all correspondence to: Murat Canpolat, Akdeniz University, School of Medicine, Department of Biophysics, Antalya, 07059, Turkey. Tel: 902-422496160; Fax: 902-422274482; E-mail: canpolat@akdeniz.edu.tr.

1083-3668/2009/14(5)/054021/7/$25.00 © 2009 SPIE

tions in the chemical composition of tissue or variations in the physical structure of tissue. Therefore, with diffuse light, correlating the changes in the acquired spectra due to absorption or scattering with tissue pathology is unlikely.

One promising technique for demarcation of tumor from surrounding normal tissue is elastic light single scattering spectroscopy (ELSSS). ELSSS detects singly scattered photons, rather than diffused photons, from tissue. Because of the small optical path length of singly scattered photons in tissue, variations in the spectrum due to the concentrations of absorbers and scatterers in the tissue are minimized.[18] The spectra of singly scattered photons therefore provide information about the size of the scatterers because this is the only parameter on which they are dependent.[18–20]

There are several ways to detect the single-scattering component of back-reflected light from a turbid medium. Detection of single-scattering components of back-reflected light is strongly related to the experimental design and the geometry of the optical fiber probe. Previously, single-scattering components of back-reflected light from tissue were obtained by modeling and subtracting the diffuse component from total back-reflected light,[19] where single-scattering components of light comprised only a small portion of the total back-reflected light and produced a low signal-to-noise ratio. Polarization light-scattering spectroscopy is another method to isolate single-scattering components of back-reflected light from diffused light.[20] The most convenient way to detect singly scattered light from a turbid medium is to use a single-fiber optical probe to deliver light to and from tissue,[18] because since this technique limits the detection of diffuse light from tissue. ELSSS spectra taken by a single-fiber optical probe using white light can quantify the size of scatterers in a tissue phantom.[18,21] Nearly 90% of single-scattering photons detected by the single-fiber optical probe originate within 200 μm of the fiber tip. Thus, the diffuse component of back-scattered light is significantly reduced.[21] Because of the small path length of singly scattered photons within tissue, the effect of the absorption by tissue chromophores on the spectral line shapes is minimized.

Several groups have been working on detecting and defining the surgical margins of high-grade gliomas intraoperatively by using spectroscopic techniques.[3,4,6–8,10,11] However, only a few studies have been performed for demarcation of low-grade tumors from surrounding normal brain tissues. Lin et al. have used fluorescence and diffuse reflectance spectroscopy for demarcation of astrocytomas and anaplastic astrocytomas in an *in vitro* study.[9] Butte et al. used time-resolved fluorescence spectroscopy to delineate meningiomas from surrounding normal tissue intraoperatively as the characteristics of intracranial meningiomas increase the difficulty of achieving complete surgical resection.[5] Therefore, new techniques need to be developed and applied to scan the surgical bed or margins of excised low-grade tumors *in situ*.

The single-fiber optical probe ELSSS system offers a new modality to detect cancerous tissue in real time.[22] The ELSSS system has been used to differentiate between malignant and benign skin lesions in an animal model. Differentiation was based on the sign of the spectral slopes, where the signs of the spectral slopes of benign and malign tissues were positive and negative, respectively.[22] This system, however, has not been tested *ex vivo* for the ability to differentiate brain tumors and surrounding normal brain tissues. In this feasibility study, a limited number of brain tissue specimens with different types of tumors and normal (white matter and gray matter) brain tissues specimens were used to test the system's efficiency in differentiating normal brain tissue and brain tumors. A detailed description of the single-fiber optical probe system is provided elsewhere.[18]

In this study, we explored the application of ELSSS for rapid intraoperative identification of brain tumors and delineation of the tumor from surrounding normal tissue based on the variation of the signs of the spectral slopes between tumor and normal brain tissues. ELSSS spectra in the wavelength range of 620–750 nm were used in brain tissue specimens to segregate tumors from surrounding normal brain tissues.

2 Material and Methods

2.1 *Sample Handling*

The pilot clinical study was conducted at Akdeniz University Hospital with the approval of the Akdeniz University Institutional Review Board. Patients undergoing brain tumor and epilepsy surgery at the Akdeniz University Neurosurgery Department were recruited regardless of gender. ELSSS data were acquired from different locations of excised brain tumors and tumor margins of 29 patients, and normal brain tissues were investigated on the margins of the tumors. The types and the number of incidences of the brain tumors encountered in the study are summarized in Table 1. Four normal white matter and four normal gray matter tissue specimens were obtained from four epilepsy patients during amygdalohippocampectomy and temporal lobectomy procedures within temporal lobes and used as a control group.

After the excision, a few drops of saline were dropped onto the brain tumor specimens to keep them moisturized during spectral data acquisition. The single-fiber optical probe was gently placed on the excised brain tissue specimens just after the excision, and spectral data acquisition was completed within 3–5 min. Illumination power of the white light at the tissue surface was 0.1 mW, and the average acquisition time of each ELSSS spectrum was 200 ms. Measurements were performed intraoperatively by the collaborating neurosurgeon.

2.2 *Instrumentation*

Elastic light single-scattering spectra of brain tissue were acquired using a system consisting of a spectrometer (USB2000 with OOIBase32TM Platinum Spectrometer Operating Software, Ocean Optics, Tampa, Florida), a tungsten halogen white-light source, a single-fiber optical probe, and a laptop computer. The single-fiber optical probe was used for both delivery and detection of white light to and from the tissue as illustrated in Fig. 1. The single-fiber optical probe was a 1×2 fiber optical coupler with a splitting ratio of 50%. One proximal end of the coupler was connected to the light source, and the other was connected to the spectrometer. The diameter of the distal end of the probe's fiber was 100 μm with a numerical aperture of 0.22.

2.3 *Experimental Methods*

ELSSS spectra were acquired from 41 brain tissue specimens. Sample sizes ranged from 2 to 125 mm^3. After the excision,

Table 1 Distribution of brain tumors.

Type of tumor tissue	Histopathological classification	Number of patients
Neuroepithelial	Astrocytic tumors	
	Pilocytic astrocytoma (WHO grade I)	3
	Diffuse astrocytoma (WHO grade II)	3
	Anaplastic astrocytoma (WHO grade III)	1
	Glioblastoma multiforme (WHO grade IV)	6
	Oligodendroglial tumors	
	Oligodendroglioma (grade II)	1
	Oligoastrocytic tumors	
	Anaplastic oligoastrocytoma (WHO grade III)	1
	Diffuse oligoastrocytoma (WHO grade II)	1
Cranial nerves	Schwannoma (WHO grade I)	2
Meninges	Meningioma (WHO grade I)	10
Sellar region	Craniopharyngioma (WHO grade I)	1

each tissue sample was placed on a black plastic sheet to prevent back reflection from the holder during the spectral data acquisition. Before acquiring the data from each tissue specimen, three spectra were measured for system calibration. The first one was a background spectrum measured from pure water by inserting the tip of the probe into water in a black container. The second spectrum was taken to define the spectral distribution of the light source, where the probe was placed nearly 1 mm above a white-light reflectance standard (Spectralon, Labsphere, Inc.) in water and the spectral distribution of the light source was measured. The last spectrum was measured from 10% aqueous suspension of monodisperse polystyrene microspheres with a diameter of 2 ± 0.5 μm to test the performance of the single-fiber optical probe.

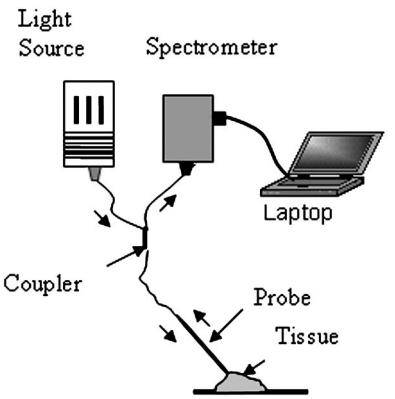

Fig. 1 Schematic of the instrumental setup for the elastic light single-scattering spectroscopy system.

We have modified the operating software of the spectrometer to change integration time automatically in order to keep the spectral intensity below a saturation value 40,000 counts and above 10,000 counts. If the maximum intensity of the tissue spectrum exceeds the saturation value of the spectrometer, the software neglects it and reduces the integration time of the spectrometer to half the original value and takes another spectrum. On the other hand, if the maximum intensity of the spectrum is $<$10,000 counts, the software increases the integration time of the spectrometer and takes a new spectrum. Each spectrum is then normalized to the integration time prior to data analysis.

The background signal was high due to back reflection of light at the fiber-water interface because of the difference between the indices of refraction of the optical fiber ($\sim$1.6) and water ($\sim$1.33) in the visible range of light. Intensity differences between the tissue spectra and background spectrum varied from 40 to -8.2%. Intensities of the spectra were calculated by integrating the area of the spectrum in the wavelength range of 620–750 nm. The intensity of the light detected from tissue changed with both the pressure between the fiber tip and tissue and with the angle of the probe and the tissue surface. Because the index of refraction of extracellular liquid (1.38) is higher than the index of refraction of water, specular back reflection at the tip of fiber is smaller in the tissue measurements than in the background measurements. Therefore, the intensity of the tissue measurements was occasionally smaller than background measurements. However, this did not affect the spectral line shape or the sign of the spectral slope.

After calibration measurements, the probe was gently placed on different sites of the tissue sample. For each site, at least 16 ELSSS spectra were obtained in the wavelength range of 350–800 nm, and the spectra were corrected in the wavelength range of 620–750 nm to calculate average spectral slopes of the brain tissue specimens. The wavelength ranges were limited due to absorption by hemoglobin of $<$620 nm and the upper limit of the visible spectrometer at 750 nm. Multiple sites within each brain tumor specimen were studied to find normal brain tissue at the tumor margins based on the signs of the spectral slopes. Normal tissue sites were investigated in each brain tumor specimen by manually scanning the surface of the tumor with the single-fiber optical probe and looking for positive spectral slopes in real time. Sites of the excised specimen with positive spectral slopes were assumed to be normal brain tissue, and those with negative spectral slopes were assumed to be tumor tissue based on our previous experiments performed using the same ELSSS system to differentiate melanoma from nonmelanoma skin tissue in an animal model.[20] After spectroscopic examination, each interrogated site was removed from the rest of the bulk tissue and then sent for histopathological examination separately. In this study, histology was used as the reference standard for tissue diagnosis. All of the normal tissue sites ob-

served at the tumor margins were white matter. To investigate the lack of detection of normal gray matter tissues at the margin of tumors, we performed a control experiment taking spectra from four normal white matter and four normal grey matter tissues obtained from four epilepsy patients.

The impact of the overhead room light on the spectral acquisition was investigated in the experiments using tissue specimens by taking spectra from the brain tissue samples while the light was on and off. The impact of the overhead room light on the spectral data was negligible. Therefore, the overhead room light was left on the during spectral data acquisition.

2.4 *Data Analysis*

The measured spectra were corrected for the wavelength dependence of system components and specular reflection. The corrected spectrum[18] is

$$R(\lambda) = \frac{R(\lambda)_s - R(\lambda)_{\mathrm{bg}}}{R(\lambda)_c - R(\lambda)_{\mathrm{bg}}}, \quad (1)$$

where, $R(\lambda)_s$ is a spectrum of the tissue, $R(\lambda)_c$ is a spectrum of Spectralon (Labsphere, Inc.) in water and $R(\lambda)_{\mathrm{bg}}$ is a background spectrum taken from pure water in a black container. Spectral data were processed in real time, and the corrected spectra were visualized on the computer screen. The single-fiber optical probe was used to record a spectrum from 10% polystyrene microspheres with a diameter of 2 ± 0.5 μm dispersed in pure water to test whether the probe could detect singly scattered photons from the tissue phantom. The observation of Mie oscillation from the spectrum of monodispersed microspheres confirmed that the ELSSS system detects single-scattered photons from turbid media rather than diffused photons.

Morphometric analysis was performed to compare the area and number density of tumoral and normal (white matter and gray matter) nuclei. Nuclear areas were determined by taking 50 measurements from each tissue site using an image analysis workstation composed of the following: a personal computer running the Microsoft Windows 98 operating system, a light microscope (Leica DMLB, Germany), a frame grabber card (Matrox Meteor, Matrox Inc., Canada), a digital camera attached to the microscope (Sony XC003P 3 CCD, Sony Inc., Japan), and image analysis software (SAMBA 2000). Average nuclear areas of 19 brain tumors, 8 normal white matter tissues, and 4 normal gray matter brain tissues were measured. Average number densities of the nuclei of white matter, gray matter, and tumor tissues were defined by counting the number of the nuclei within a window of 200×200 image pixels in four different locations on the images. Total image size was 575×767 pixels and obtained at $400\times$ magnification by the light microscope.

3 Results

Of the 41 total sites that underwent spectroscopic analysis, 16 were classified histologically as grade I tumors, 5 as grade II tumors, 2 as grade III tumors, 6 as grade IV tumors, and 12 as normal brain tissue with eight white matter and four gray matter samples. There were 21 instances of low-grade tumors (grades I and II) and 8 high-grade tumors. Tumors were classified based on World Health Organization (WHO) criteria.

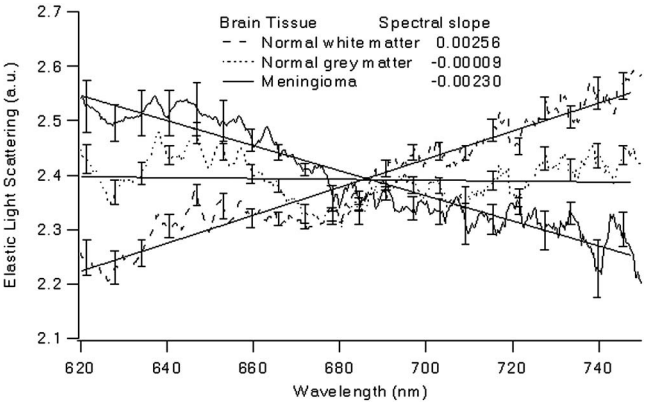

Fig. 2 Corrected spectra of normal white matter, normal gray matter, and meningioma tumor brain tissues.

All spectra were corrected using Eq. (1). There was a significant difference between the corrected spectra of the tumors and normal white matter detected at the margins of the excised tumors. Spectral slopes of tumors were negative, and spectral slopes of white matter tissue specimens were positive. Only two tumors were misclassified as normal brain tissue. One of them was a grade I tumor: pilocytic astrocytoma. The other one was a grade III tumor: anaplastic oligoastrocytoma. Four white matter brain tissue sites were detected with spectroscopic analysis from the margins of four tumors and verified by histopathological examination. One of the white matter tissue sites was found at the margin of a grade IV tumor, and the other three were found at the margins of grade II tumors. The grade II tumors were oligodendroliom, diffuse oligoastrocytoma, and diffuse astrocytoma.

We were expecting to find normal gray matter sites during interrogation of normal tissues at the margins of excised brain tumors using the ELSSS system as well, but none were observed. Therefore, we performed a control experiment to investigate whether there is a difference between the spectra of normal white matter and normal gray matter. The spectral slopes of three of four gray matter specimens were negative, and one was positive. Spectral slopes of the four normal white matter specimens were positive as expected. Average spectra of normal white matter, normal gray matter, and meningioma tumor tissues are shown in Fig. 2. The corrected spectrum of normal white matter tissue has a positive slope, and the spectrum of the meningioma tumor and normal gray matter tissues have negative slopes. This may account for the inability to detect normal gray matter at the margins of tumors using the sign of the spectral slope as a discrimination parameter.

We have investigated the inability to discriminate normal gray matter brain tissue from brain tumors by comparing histopathology pictures of normal white and gray matter tissues with a brain tumor tissue, oligoastrositoma. As shown in Figs. 3(a) and 3(b), oligoastrositoma tumor cells have larger nuclei, are more irregular, and have higher ratios of nuclear to cytoplasmic volume than cells in the surrounding normal white brain tissue. The nuclear size distribution of normal gray matter is large, as seen in Fig. 3(c), where neurons have large nuclei and glial cells have small nuclei. The average nuclear

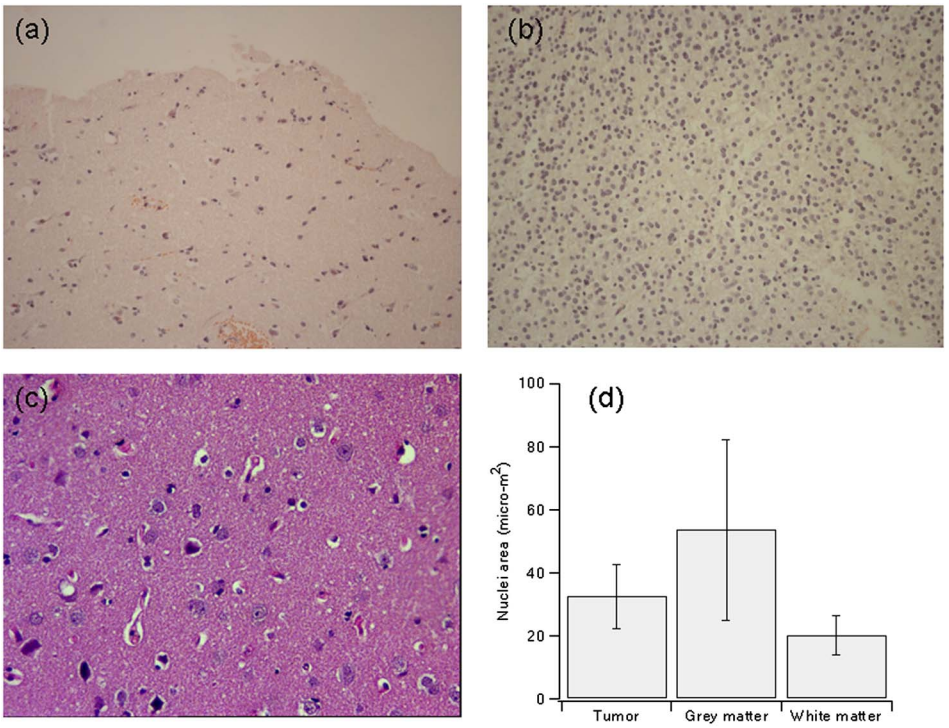

Fig. 3 (a) Histological appearance of normal white matter brain tissue. There was no evidence of cancer cells, H&E X 200. (b) Histological appearance of gray matter. Large nuclei belong to nerve cells. There is a large diversity in the size of nuclei, H&E X 200. (c) H&E staining of diffuse oligoastrositoma tumor tissue that has eosinophilic cytoplasm and hyperchromatic nuclei with prominent eosinophilic nucleoli. (d) Average area of normal white matter, normal gray matter, and tumor cell nuclei.

area of normal gray matter is larger than the average nuclear area of oligoastrositoma tumors as seen in the histogram [Fig. 3(d)]. The average nuclear areas of tumors, normal white matter, and normal gray matter were calculated over 20, 8, and 4 brain tissue samples, respectively. There is a statistically significant difference between the average size of nuclei of normal white matter and the average sizes of nuclei in tumor and normal gray matter tissues, $p < 0.005$.

The distribution of the spectral slopes of tumors, normal white matter, and normal gray matter are shown in Fig. 4. The sensitivity and specificity of the system were measured by comparing the signs of the spectral slopes to the histopathological results. The sign of the spectral slope is negative for three of the four normal gray matter samples and positive for one. The ELSSS system correctly defined 27 of 29 tumors and defined four normal white matter sites, as well. Discrimination of normal white matter brain tissue from high- and low-grade tumors using the sign of the spectral slopes results in a sensitivity of 93% and a specificity of 100%, but the ELSSS system is unable to differentiate gray matter from tumors based on the sign of the spectral slopes. Since only one low-grade tumor was misclassified out of 21 samples, the sensitivity and specificity for the discrimination of low grade tumors from the surrounding white matter are 95 and 100%, respectively.

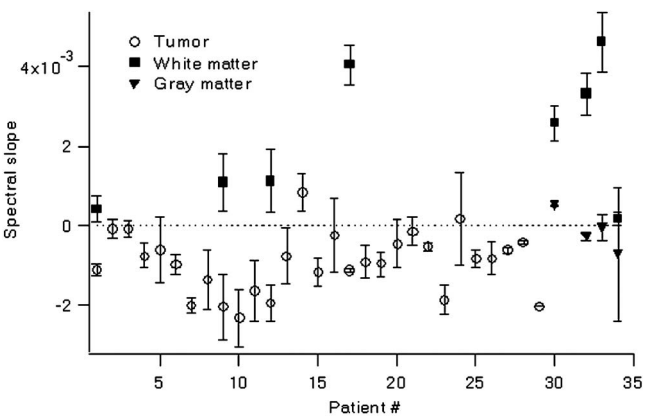

Fig. 4 Spectral slopes of tumor and normal tissues. Tissues are classified based on the spectral slopes. If the slope is greater than zero, then the tissue is classified as normal; otherwise, it is classified as tumor.

4 Discussion and Conclusions

Light scatters in a medium due to heterogeneity in the index of refraction of the medium. The index of refraction for cell membranes is greater than the index of refraction for extracellular liquid, which causes scattering of light at the cell membrane. Light also scatters inside a cell at the nucleus, mitochondria, and other organelles due to difference in the index of refraction between intracellular compartments and the surrounding cytoplasm. Most of the scattering from the cells takes place due to structures within the cells.[23] The average refractive indices of the cytoplasm and membranes of the cells and organelles are 1.38 and 1.48, respectively.[24]

The cause of the difference between the sign of the spectral slopes between normal white matter, normal gray matter, and

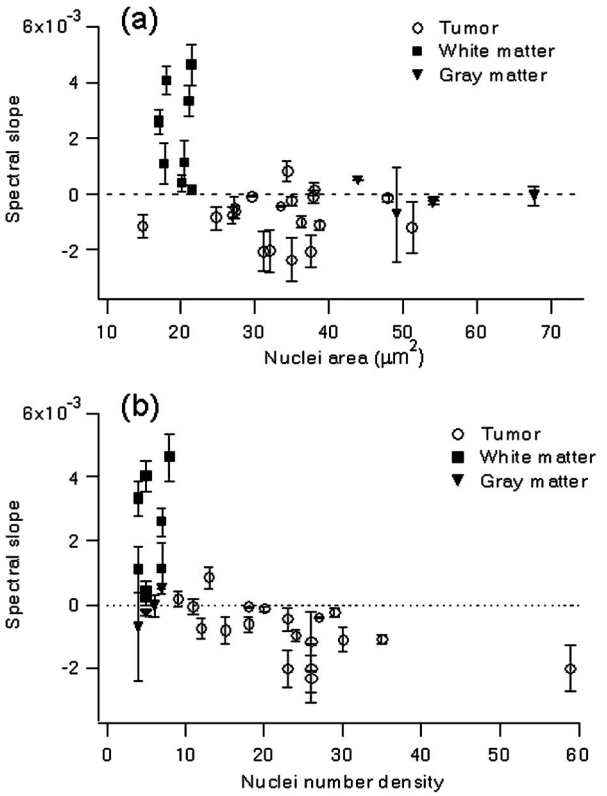

Fig. 5 (a) The sign of the spectral slopes is positive for small nuclear area and negative for large nuclear area. (b) Normal white matter and normal gray matter have similar number densities, but the signs of their spectral slopes differ. There is no correlation between sign of the spectral slope and number density.

tumor tissues was investigated by comparing morphometric features of the nuclei. The average size of nuclei and the number density of nuclei in those three tissues are different, as shown in Fig. 3. In addition to the enlargement of nuclei in tumor tissue, the density and close packing of nuclei is increased compared to normal white matter tissue. On the other hand, the average size of nuclei in gray matter is larger than in tumors, but the number density of nuclei in gray matter is smaller than that of tumors, as shown in Fig. 3(d). Therefore, variation of the spectral slope is analyzed with respect to nuclear size and number density as shown in Fig. 5. The spectral slope is positive for small nuclear area (normal white matter) and negative for large nuclear area (tumor) in Fig. 5(a). In the same figure, the spectral slopes of three out of four normal gray matter tissue specimens are negative and one is positive. This indicates that negative spectral slope is correlated with large nuclei and positive spectral slope is correlated with small nuclei in cells. Variation of the spectral slope with respect to the number density of nuclei is shown in Fig. 5(b). The number densities of normal white matter and normal gray matter are similar, and both values are lower than the number density of the tumors. In contrast, the sign of the spectral slopes of most of the gray matter is negative as is the case for tumors. This indicates that the signs of the spectral slopes change with nuclear size, but not with number density of the nuclei in brain tissues.

Normal white matter brain tissues and brain tumors were differentiated based on the signs of the spectral slopes of the ELSSS spectra. To the best of our knowledge, there is no analytical model to explain marked differences in spectral slopes of normal and tumoral tissues based on the size of the scatterers. However, there are similarities between our experimental results and the computational model of light scattering in normal and precancerous cervical cells reported elsewhere. In one such study,[25] Drezek et al. used a simulation model based on a heterogeneous population of cells, including both normal and precancerous cervical cells. Light scattering from cells was calculated by a pulsed finite-difference time-domain method. In the simulation, broadband light in the range of 600–1000 nm was used. Intensity of the scattered light was integrated as a function of wavelength for different scattering angular ranges. The contrast between the integrated intensities of normal and precancerous cells was most apparent for the angular range of 160–180 deg. The intensity of scattered light increased with wavelength for normal cells, but did not change for dysplasia. A notable similarity occurred between the ELSSS spectra of our *ex vivo* experiments and the spectra calculated in this simulation. Our experimental results showed that backscattered light intensity increased with wavelength for normal white matter and decreased for tumors. This resembles the observations in Drezek's simulation. Because the numerical aperture of the optical fibers used in our probe is 0.22, the half-acceptance angle of the light is 13 deg. The back-reflected light in the angular range of 167–180 deg collected by the single optical fiber probe in our light collection geometry is similar to the geometry described in Drezek's study.

The intensity of light collected by the single-fiber optical probe is defined by the size distribution of the scatterers, the relative index of refraction of scatterers to surrounding medium, the wavelength of light, and the numerical aperture of the single-fiber optical probe. Intensity of light detected by the single-fiber optical probe as a function of wavelength is

$$2\left(\frac{\pi}{k^2}\right)\int_{167}^{180}[|S_1(\vartheta)|^2+|S_2(\vartheta)|^2]\sin\vartheta d\vartheta, \qquad (2)$$

where k is wave number of light, ϑ is the angle, and S_1, S_2 are scattering amplitudes in Mie theory.[26] As seen in Eq. (2), the intensity of detected light is proportional to the integral of scattering amplitude in the angular range of the acceptance angle of the single-fiber optical probe. Therefore, spectral distribution of back-reflected light is defined not only by the tissue, but also by the numerical aperture of the single-fiber optical probe. Calculating the intensity of singly scattered photons as a function of wavelength using Eq. (2) requires knowledge of the size distribution of scatters in normal and cancerous tissues.

The identification of margins of malignant gliomas using exogenous fluorescence molecules, such as fluorescein, or precursors, such as 5-aminovelunic acid, has been successfully demonstrated.[7,27–29] However, only a few studies have been performed on the demarcation of low-grade tumors from normal brain tissue.[5] This *ex vivo* study shows that the ELSSS system has the potential to differentiate high- and low-grade brain tumors from normal white matter brain tissues. How-

ever, the ELSSS system cannot provide detailed information about tissue and cannot replace histopathology. The resolution of the ELSSS system is lower than microscopy.

Only one single-fiber optical probe was used to deliver and detect light to and from tissues in this study. Because the diameter of the single-fiber optical probes was 100 μm, inspecting the complete surgical bed requires much time, and is not clinically feasible. Therefore, we are currently constructing a 7×7 array of single-fiber optical probes to scan a 25-mm^2 tissue surface systematically with a resolution of 0.7 mm within 1 min.

Most glioma tumors originate within subcortical white matter, rather than in gray matter, and the speed of advance of tumor margins across white matter is two to three times faster than across gray matter;[30] therefore the probability of having a tumor in white matter is greater than that of having a tumor in gray matter. Hence, the single-fiber optical probe ELSSS system has the potential to be used as an adjunctive tool for intraoperative rapid detection of low- and high-grade brain tumors and demarcation of the tumors from surrounding normal white matter tissue *in vivo*. Detecting positive surgical margins may improve the overall survival rate of patients with brain tumors after surgery.

Acknowledgments

This work was supported, in part, by EU Grant No. MIRG-CT-2006-046565 and, in part, by Akdeniz University Scientific Research Units, Antalya, Turkey. The authors are grateful to Dr. Caner Özbey for his technical assistance on defining the area of nuclei.

References

1. T. Arbel, X. Morandi, R. M. Comeau, and D. L. Collins, "Automatic non-linear MRI-ultrasound registration for the correction of intra-operative brain deformations," *Comput. Aided Surg.* **9**(4), 123–136 (2004).
2. L. M. Auer and V. van Velthoven, "Intraoperative ultrasound imaging: comparison of pathomorphological findings in US and CT," *Acta Neurochir. Suppl. (Wien)* **104**(3–4), 84–95 (1990).
3. A. Bogaards, A. Varma et al., "Increased brain tumor resection using fluorescence image guidance in a preclinical model," *Lasers Surg. Med.* **35**, 181–190 (2004).
4. A. C. Croce, S. Fiorani, D. Locatelli, R. Nano, M. Ceroni, F. Tancioni, E. Giombelli, E. Benericetti, and G. Bottiroli, "Diagnostic potential of autofluorescence for an assisted intraoperative delination of glioblastoma resection margins," *Photochem. Photobiol.* **77**, 309–318 (2003).
5. P. V. Butte, B. K. Pikul, A. Hever, W. H. Yong, K. L. Black, and L. Marco, "Diagnosis of meningiomas by time-resolved fluorescence spectroscopy," *J. Biomed. Opt.* **10**(6), 1–9 (2005).
6. L. M. Arcu, J. A. Jo, P. V. Butte, W. H. Yong, B. K. Pikul, K. L. Black, and R. C. Thompson, "Fluorescence lifetime spectroscopy of glioblastoma multiforme," *Photochem. Photobiol.* **80**, 98–103 (2004).
7. W. Stummer, U. Pichlmeier, T. Meinel, O. D. Wiestler, F. Zanella, H.-J. Reulen et al., "Fluorescence-guided surgery with 5-aminolevunic acid for resection of malignant glioma: randomised controlled multicentre phase III trial," *Lancet Oncol.* **7**, 392–401 (2006).
8. S. C. Gebhart, W. C. Lin, and A. Mahadevan-Jansen, "*In vitro* determination of normal and neoplastic human brain tissue optical properties using inverse adding-doubling," *Phys. Med. Biol.* **51**, 2011–2027 (2006).
9. W.-C. Lin, S. A. Toms, M. Motamedi, E. D. Jansen, and A. Mahadevan-Jansen, "Brain tumor demarcation using optical spectroscopy: an *in vitro* study," *J. Biomed. Opt.* **5**(2), 214–221 (2000).
10. S. A. Toms, W.-C. Lin, R. J. Weil, M. D. Johnson, E. D. Jansen, and A. Mahadevan-Jansen, "Intraoperative optical spectroscopy identifies infiltrating glioma margins with high sensitivity," *Neurosurgery* **57**, 382–391 (2005).
11. J. Shinoda, H. Yano, S. Yoshimura et al., "Fluorescence-guided resection of glioblastoma multiforme by using high-dose fluorescein sodium: technical note," *J. Neurosurg.* **99**, 597–603 (2003).
12. J. R. Mourant, I. J. Bigio, J. Boyer, T. M. Johnson, J. Lacey, A. G. Bohorfoush, and M. Mellow, "Elastic scattering spectroscopy as a diagnostic tool for differentiating pathologies in the gastrointestinal tract: preliminary testing," *J. Biomed. Opt.* **1**, 192–199 (1996).
13. Z. Ge, K. T. Schomacker, and N. S. Nishioka, "Identification of colonic dysplasia and neoplasia by diffuse reflectance spectroscopy and pattern recognition techniques," *Appl. Spectrosc.* **52**, 833–839 (1998).
14. G. Zonios, L. T. Perelman, V. Backman, R. Manoharan, M. Fitzmaurice, J. V. Dam, and M. S. Feld, "Diffuse reflectance spectroscopy of human adenomatous colon polyps *in vivo*," *Appl. Opt.* **38**, 6628–6637 (1999).
15. M. Mehrubeoglu, N. Kehtarnavaz, G. Marquez, M. Duvic, and L. V. Wang, "Skin lesion classification using oblique-incidence diffuse reflectance spectroscopic imaging," *Appl. Opt.* **41**, 182–192 (2002).
16. I. J. Bigio and S. G. Bown, "Spectroscopic sensing of cancer and cancer therapy," *Cancer Biol. Therapy* **3**, 259–267 (2004).
17. O. M. A'Amar, R. D. Ley, and I. J. Bigio, "Comparison between ultraviolet-visible and near-infrared elastic scattering spectroscopy of chemically induced melanomas in an animal model," *J. Biomed. Opt.* **9**(6), 1320–1326 (2004).
18. M. Canpolat and J. R. Mourant, "Particle size analysis of turbid media with a single optical fiber in contact with the medium to deliver and detect white light," *Appl. Opt.* **40**, 3792–3799 (2001).
19. L. T. Perelman, V. Backman, M. Wallace, G. Zonios, R. Manoharan, A. Nusrat, S. Shields, M. Seiler, C. Lima, T. Hamano, I. Itzkan, J. Van Dam, J. M. Crawford, and M. S. Feld, "Observation of periodic fine structure in reflectance from biological tissue: a new technique for measuring nuclear size distribution," *Phys. Rev. Lett.* **80**, 627–630 (1998).
20. V. Backman, R. Gurjar, K. Badizadegan, I. Itzkan, R. R. Dasari, L. T. Perelman, and M. S. Feld, "Polarized light scattering spectroscopy for quantitative measurement of epithelial cellular structures *in situ*," *IEEE J. Sel. Top. Quantum Electron.* **5**, 1019–1026 (1999).
21. A. Amelink, M. P. L. Bard, S. A. Burgers, and H. J. C. M. Sterenborg, "Single-scattering spectroscopy for the endoscopic analysis of particle size in superficial layers of turbid media," *Appl. Opt.* **42**, 4095–4101 (2003).
22. M. Canpolat, A. G. Gökhan, M. A. Çiftçioğlu, N. Erin, "Differentiation of melanoma from non-cancerous tissues in an animal model using elastic light scattering spectroscopy," *Technol. Cancer Res. Treat.* **7**, 235–240 (2008).
23. J. Beuthan, O. Mine, J. Helfmann, M. Herrig, and G. Muller, "The spatial variation of the refractive index in biological cells," *Phys. Med. Biol.* **41**, 369–382 (1996).
24. J. R. Mourant, J. P. Freyer, A. H. Hielsher, A. A. Eick, D. Shen, and M. Johnson, "Mechanism of light scattering from biological cells relevant to noninvasive optical-tissue diagnostics," *Appl. Opt.* **37**, 3586–3593 (1998).
25. R. Drezek, A. Dunn, and R. Richards-Kortum, "A pulsed finite-difference time-domain method for calculating light scattering from biological cells over broad wavelength ranges," *Opt. Express* **6**, 147–157 (2000).
26. C. F. Bohren and D. R. Huffman, *Absorption and Scattering of Light by Small Particles*, Wiley, Hoboken, NJ (1998).
27. W. Stummer, S. Stocker, S. Wagner, H. Stepp, C. Fritsce, C. Goetz, A. Goetz, R. Kiefmann, and H. Reulen, "Intraoperative detection of malignant gliomas by 5-aminolevulinic acid-induced porphyrin fluorescence," *Neurosurgery* **42**(3), 518–526 (1998).
28. W. Stummer, A. Novotny, H. Stepp, C. Goetz, K. Bise, and H. J. Reulen, "Fluorescence-guided resection of glioblastoma multi-forme by using 5-aminolevunic acid-induced porphyrins: a prospective study in 52 consecutive patients," *J. Neurosurg.* **93**, 1003–1013 (2000).
29. A. Zimmermann, M. Ritsch-Marte, and H. Kostron, "mTHPC-mediated photodynamic diagnosis of malignant brain tumors," *Photochem. Photobiol.* **74**(4), 611–616 (2001).
30. K. R. Swanson, C. Bridge, J. D. Murray, and E. C. Alvord, Jr., "Virtual and real brain tumors: using mathematical modeling to quantify glioma growth and invasion," *Semicond. Int.* **216**, 1–10 (2003).